


Article

Estimation of China's Contribution to Global Greening over the Past Three Decades

Jing Peng ^{1,*} , Fuqiang Yang ¹, Li Dan ¹ and Xiba Tang ²

¹ CAS Key Laboratory of Regional Climate-Environment for Temperate East Asia, Institute of Atmospheric Physics, Chinese Academy of Sciences, Beijing 100029, China; yangfq@tea.ac.cn (F.Y.); danli@tea.ac.cn (L.D.)

² Laboratory of Cloud-Precipitation Physics and Severe Storms (LACS), Institute of Atmospheric Physics, Beijing 100029, China; tangxb_6@mail.iap.ac.cn

* Correspondence: pengjing@tea.ac.cn

Abstract: China's contribution to global greening is regulated by increasing atmospheric CO₂ concentrations, climate change, and land use. Based on TRENDY project data, this study identified that the shifts in China's contribution to the global leaf area index (LAI) trend strongly reduced during the warming hiatus, translating from $13.42 \pm 26.45\%$ during 1982–1998 into $7.91 \pm 25.45\%$ during 1999–2012. First, significant negative sensitivities of LAI to enhanced vapor pressure deficit (VPD), when only considering the climate effect derived from TRENDY models in China, were found to have shifted substantially after the late 1990s. However, globally, LAI had positive rather than negative responses to enhanced VPD. These opposing shifts in the response of LAI to enhanced VPD reduced the national contribution to global vegetation greening. Second, shifts in land-use change and their effects on the LAI trends in the two periods in China were accompanied by major changes in land cover and land management intensity, including forestry. Consequently, the contribution of land use in China reduced by -47.68% during the warming hiatus period, as compared with the warming period. Such a shift in the impact of land-use change on LAI simulated by ecosystem models might result from the models' lack of consideration of conserving and expanding forests with the goal of mitigating climate change for China. Our results highlight the need for ecosystem models to reproduce the enhanced negative impact on global LAI and consider the shifts in man-made adaptation policies (e.g., forest management) to improve terrestrial ecosystem models in the future.

Keywords: leaf area index; vapor pressure deficit; climate change; land-use change; ecosystem model



Citation: Peng, J.; Yang, F.; Dan, L.; Tang, X. Estimation of China's Contribution to Global Greening over the Past Three Decades. *Land* **2022**, *11*, 393. <https://doi.org/10.3390/land11030393>

Academic Editors: Baojie He, Ayyoob Sharifi, Chi Feng and Jun Yang

Received: 17 February 2022

Accepted: 21 February 2022

Published: 8 March 2022

Publisher's Note: MDPI stays neutral with regard to jurisdictional claims in published maps and institutional affiliations.



Copyright: © 2022 by the authors. Licensee MDPI, Basel, Switzerland. This article is an open access article distributed under the terms and conditions of the Creative Commons Attribution (CC BY) license (<https://creativecommons.org/licenses/by/4.0/>).

1. Introduction

For about three decades, from 1982 to 2009, the global leaf area index (LAI) trend was estimated at $0.068 \pm 0.045 \text{ m}^2 \text{ m}^{-2} \text{ yr}^{-1}$ (mean \pm standard deviation, 1 sigma) [1]. This generally increasing trend since 1982 would have shifted urban energy balance and regulated land–atmosphere interactions, including sensible heat fluxes, evapotranspiration, carbon dioxide (CO₂) exchange between land and atmosphere, and other trace gases and aerosols [2–4]. Furthermore, the changes in LAI since the 1980s are likely to have affected land–surface boundary conditions and influenced the surface albedo, roughness, and even the dynamics of the terrestrial water cycle [5]. The modulated energy and water cycles caused by changes in LAI might partly have yielded changes in the terrestrial carbon balance [6,7] and atmospheric chemistry through emissions and deposition of CO₂ and other trace gases and aerosols [8]. Therefore, tracking and understanding trends in LAI is central to predicting climate change and quantifying the carbon budgets of terrestrial ecosystems [9].

The increasing atmospheric CO₂ concentration exerts a first-order control on the increasing LAI trend. At the regional scale, meanwhile, a strong control of vegetation greening by increased surface air temperature has been shown in relatively temperature-limiting conditions based on satellite remote sensing data [1,10]. Several lines of evidence show

enhanced vegetation greening over the past few decades with medium or high confidence using satellite-derived vegetation datasets [1,11]. However, the observation-driven inference of increasing LAI has been based mostly on enhanced atmospheric warming in the high latitudes of the Northern Hemisphere [10], along with dynamic global vegetation model (DGVM)-simulated increases in photosynthesis [5] in the northern extra-tropics [11]. The increased LAI trend may also have benefited from human land-use management in the form of intensive ecosystem management [12]. Among these factors, there needs to be an emphasis on how to accurately reproduce their influences in earth system models—an aspect still requiring continuous efforts [5,13].

The so-called “global warming hiatus”, which is broadly regarded as having started in around 1998 and ended around 2012, was a period when the annual mean global air temperature did not seem to increase as much as expected given the increasing concentrations of atmospheric greenhouse gases [14]. Moreover, despite accumulating evidence of an increased carbon sink since 1998, there is uncertainty surrounding the key mechanism involved in such changes. While Ballantyne et al. [15] observed accelerating net terrestrial carbon uptake during the warming hiatus due to reduced respiration, Piao et al., (2018) [6] showed that the decreasing land-use emissions may have been responsible for the increased terrestrial net carbon sink during this period. Conversely, according to satellite product data, vegetation greening during the warming hiatus stalled after 1998 at the global scale [16,17], as the vapor pressure deficit (VPD) drove transpiration, which controlled leaf stomata and affected soil and plant-tissue water content [13]. Uncertainties remain regarding the magnitude of LAI trends at the regional scale based on DGVMs or satellite datasets because of the nonlinear relation between regional and global LAI trends [1,10,18].

Changes in climatic variables over the last three decades show widespread differences at the global scale. For example, increasing trends in VPD in the globe possibly influence plant growth, chemical composition, and soil respiration [13]. So, China’s contribution to global LAI may generally depend on climatic variables. The primary objective of this study, therefore, was to quantify the differences in China’s contribution to global vegetation greening between two periods—one a warming period from 1982 to 1998 and the other the warming hiatus from 1999 to 2012—and to estimate the contributions of different factors (e.g., climate change, rising atmospheric CO₂, and land-use changes) to China’s overall contribution to the global LAI trend. For a better understanding of the mechanisms driving China’s contribution to global vegetation greening, we used 13 models from the Net Land–Atmosphere Exchange Trends Project (TRENDY) (Tables 1 and 2) and two satellite-based products. Through comparison of the relative contributions (i.e., CO₂ fertilization, climate, and land use) with ecosystem vegetation growth during the global warming hiatus and warming period, we examined whether terrestrial ecosystem models can adequately capture the observed contribution of China to the global LAI trends after the late 1990s, based on results from these 13 models.

The rest of the paper is structured as follows: Section 2 describes the methods and data, including the 13 terrestrial ecosystem models and two satellite-based products used in this study. Section 3 presents the results. Section 4 provides some discussion points, followed in Section 5 by our conclusions.

Table 1. The 13 TRENDY models used in this study.

Model Names	Abbreviation	NC	Fire	WH	SC	NF	Ref.
CABLE-POP	CAB	Y	N	Y	Y	N	[19]
CLASS-CTEM	CLA	Y	Y	N	N	N	[20]
IBIS	IBI	Y	Y	Y	Y	Y	[16]
ISAM	ISA	Y	N	Y	N	Y	[21]
ISBA	ISB	Y	Y	N	N	N	[22]
JULES	JUL	Y	N	N	N	N	[23]
LPJ	LPJ	Y	Y	Y	Y	Y	[24]
LPX	LPX	Y	Y	Y	Y	N	[25]
ORCHIDEE	ORC	Y	N	Y	N	N	[26]
SDGVM	SDG	Y	Y	N	N	N	[27]
VISIT	VIS	Y	Y	Y	Y	N	[28]
YIBs	YIB	Y	Y	Y	N	N	[29]
CLM5.0	CLM	Y	Y	Y	Y	Y	[25]

Note: For each TRENDY model, it is specifically indicated whether they considered a full nitrogen cycle (NC), simulated fire and included wood harvesting (WH), shifting cultivation (SC), or nitrogen fertilization (NF). Le Quéré et al. [30] provides a complete explanation of the processes for each model.

Table 2. Used abbreviations in this study.

Full Name	Abbreviation
Leaf area index	LAI
Surface air temperature	SAT
Precipitation	PR
Vapor pressure deficit	VPD
Solar radiation	SRAD
Specific humidity	q
Surface atmospheric pressure	P_s
Dynamic global vegetation model	DGVM
Trends in the Land Carbon Cycle Project	TRENDY
Land-use change	LUC
Trends	TRE
Inter-annual variability	IAV
Mean	MEA

2. Data and Methods

2.1. Simulated and Satellite-Based Datasets

This study used the monthly LAI outputs of the Trends in the Land Carbon Cycle Project (TRENDY) [31]. Although the processes and parameterizations of the models that participated in the TRENDY project were different from those related to the LAI calculation, they were all driven by the same CRUNCEP climate reconstruction datasets [32]. The simulated period covered 1700 to 2019. Among the TRENDY experiments, there were four different types as follows: (1) S0: control. No forcing change (time-invariant “pre-industrial” CO₂ and climate and land-use mask). S0 is needed to diagnose any “cold start” issues or model drift; (2) S1: CO₂ only (time-invariant “pre-industrial” climate and land-use mask); (3) S2: CO₂ and climate only (time-invariant “pre-industrial” land use mask); (4) S3: CO₂, climate, and land use (all forcing time-varying). Simulation S0 fixes atmospheric CO₂ (276.59ppm ppm), climate (climate mean during 1901–1920), and land-use change (1700 constant level) at the pre-industrial level. Transient simulations cover the period of 1901–2018, which includes varying CO₂ (S1, S2, and S3), 1700 CO₂ (S0), varying climate (S2 and S3), varying land-use change (S3), and 1700 land-use change (S0, S1, and S2). To date, the simulations of the TRENDY project have been widely used to analyze terrestrial carbon budgets at both regional and global scales [33–35].

To illustrate the LAI trends driven by different factors, we used simulations S1 minus S0 to characterize the effect of CO₂ concentration; simulations S2 minus S1 to describe the effect of climate change; and simulations S3 minus S2 to represent the impact of land-

use change. It should be noted that not all models could simulate processes related to land-use change. For example, only some models considered processes such as wood and crop harvesting, N fertilization, irrigation, or crop rotation [31,36]. At the same time, the input land-cover dataset had a discontinuity problem in the last decade, and different models might have made different assumptions when converting the original land-use coordination dataset into a model-specific land-cover input. Therefore, the differences between simulations S3 and S2 could only partially represent the impact of land-use change in the last decade [6]. In addition, all outputs from ecosystem models were regridded to a common spatial resolution of $0.5^\circ \times 0.5^\circ$ based on bilinear interpolation.

Two satellite-observed LAI products (GIMMS LAI and GLASS LAI) were used to analyze the changes in global vegetation for the period of 1982–2012, covering the globe with a spatial resolution of $0.5^\circ \times 0.5^\circ$. These products have been validated as research-quality datasets [4] and used extensively in research on long-term vegetation dynamics [4,5,31,37]. To examine China's contribution to the global LAI trend, we calculated the LAI of each pixel in China and weighted the results by the area of each pixel. From 1982 to 2012, we used the area-weighting during the growing season from April to September to calculate the changes in LAI of the globe and China based on these remote sensing products. In addition, the warming (1982–1998) and warming hiatus (1998–2012) periods were segmented to compare the shift in China's contribution from one period with the next.

2.2. Methods

The VPD used in this study was calculated from the surface air temperature, surface atmospheric pressure, and specific humidity [38], as follows:

$$\text{VPD} = 6.1094 \times \exp\left(\frac{17.625 \times \text{SAT}}{\text{SAT} + 243.04}\right) - \frac{P_s}{0.622} \times q \quad (1)$$

where P_s is the near-surface atmospheric pressure (unit: hPa), q is the specific humidity (unit: kg kg^{-1}) and SAT is the near-surface air temperature (unit: $^\circ\text{C}$).

Monthly surface air temperature, precipitation, surface atmospheric pressure, and specific humidity and net solar radiation from the CRUNCEP datasets, which is used as atmospheric forcing data for the Community Land Model (<https://data.ucar.edu/dataset/cruncep-version-7-atmospheric-forcing-data-for-the-community-land-model> (accessed on 17 February 2022)), were employed to derive their coupled relationships with the vegetation variability. The trends in LAI were calculated during the study periods based on linear least-squares regression analysis. We estimated the responses of LAI to surface air temperature, precipitation, and VPD over the past three decades using a linear regression approach. The Mann–Kendall test was used to assess the statistical significance of the trends. A linear regression approach was further used to quantify the climate sensitivity of LAI to the precipitation, surface air temperature, or VPD. This method was applied by Poulter et al. [39] as follows:

$$y = \beta_i x + \varepsilon_i, \quad (2)$$

where x is precipitation, surface air temperature, or VPD; y is LAI; β_i is the climate sensitivity of LAI to these climatic variables; and ε_i is an error term.

Based on the contribution of each grid point in China, China's contribution to the global LAI trend could be further summarized. In this respect, we adopted an index [33] to calculate the sign and magnitude of the contribution of each grid point to the global LAI trend, as follows:

$$f_j = \frac{x_j |X|}{|X|} \quad (3)$$

where x_j is the product of the LAI trend and area for the j th grid point or j th region during the study period and X is the product of the global LAI trend and areas, such that $X = \sum x_j$. By this definition, f_j is the average relative trend of x_j/X for the j th grid point or the j th region, weighted with the absolute global trend $|X|$. Regions or grid points receiving

higher and positive average scores are inferred to be making a larger contribution to global greening. The index we adopted enabled a comparison of their relative importance (contributions) in governing global LAI greening.

3. Results

3.1. Estimates of LAI Trends under Two Conditions

The global-mean LAI experienced an increase from 1982 (Figure 1). The 14 years from 1999 to 2012 showed slightly smaller growth in the global LAI trend compared with that from 1982 to 1998, according to the TRENDY ensemble (Figure 1a). The LAI in China showed an evidently smaller increasing trend as simulated by TRENDY during the period of 1999–2012, compared with the trend for the globe. A general increasing trend for LAI in China of $0.003 \pm 0.013 \text{ m}^2 \text{ m}^{-2} \text{ yr}^{-1}$ ($p = 0.02$) during the warming hiatus was simulated by the TRENDY ensemble, while a relatively greater increasing trend of $0.007 \pm 0.03 \text{ m}^2 \text{ m}^{-2} \text{ yr}^{-1}$ ($p < 0.01$) was estimated from 1982 to 1998 (Figure 1). Compared with the remote sensing data, the trend in LAI for China during the latter period tended to be underestimated by the TRENDY ensemble. In contrast, the LAI trend using remote sensing data during 1999–2012 was greater for China by $0.023 \pm 0.011 \text{ m}^2 \text{ m}^{-2} \text{ yr}^{-1}$ than that for the globe by $0.005 \pm 0.002 \text{ m}^2 \text{ m}^{-2} \text{ yr}^{-1}$.

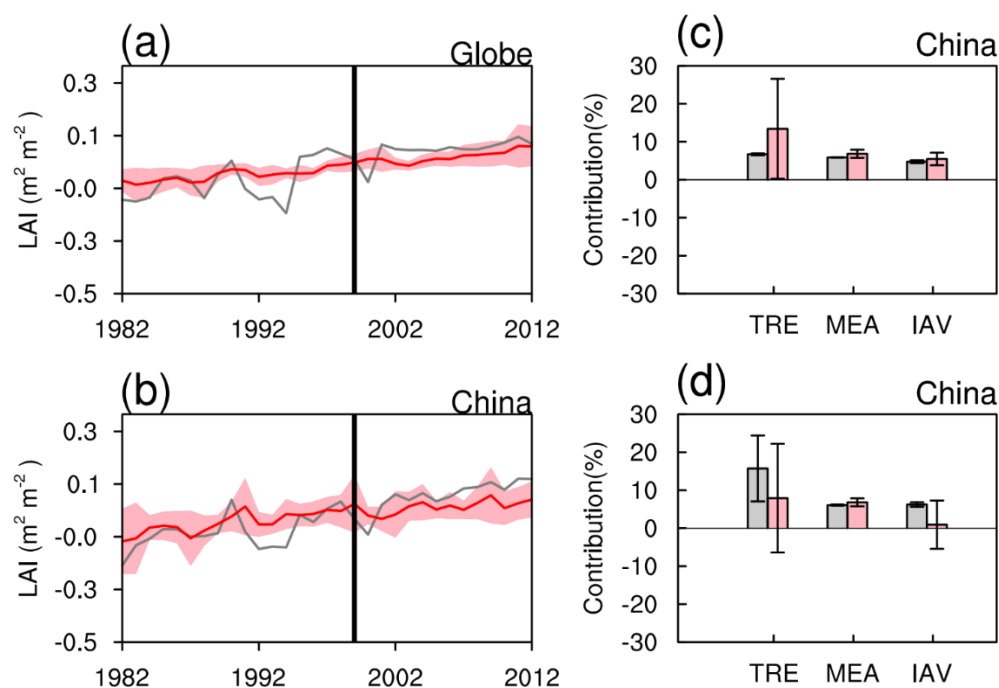


Figure 1. (a,b) Interannual anomalies of LAI in the growing season (April–September) during the period of 1982–2012 from satellite-based datasets (gray line) (GIMM LAI and GLASS LAI) and the mean of TRENDY models (red line). Shaded pink areas designate ± 1 standard deviation (σ). The left of the thick black vertical line represents the warming period from 1982 to 1998, while the right represents the warming hiatus period from 1999 to 2012 for the whole terrestrial ecosystem and China, respectively.

(c,d) Contribution of China to the global mean, trend, and interannual variability of LAI during (c) the period of 1982–1998 and (d) 1999–2012. Horizontal lines indicate $\pm\sigma$. Gray bars mean the average of satellite-based datasets; pink bars represent TRENDY ensemble (TRE: the trend of LAI; MEA: the mean of LAI; IAV: inter-annual variability of LAI).

These differences between ecosystem models and satellite-based products in the changes in China’s contribution to the global mean, trend, and interannual variability (IAV) in LAI correspond in various ways to the different periods (Figure 1c,d). Over the warming period from 1982 to 1998, the TRENDY ensemble simulated China’s contribution to the

global LAI trend to be $13.42 \pm 26.45\%$, while the observed contribution based on remote sensing data was $6.71 \pm 3.71\%$. Between the two data sources, China's contribution to the global mean and IAV derived from the TRENDY ensemble was 6.84% and 5.46%, respectively, whereas the satellite-based products predicted a smaller contribution to the IAV, at 5.89%, as well as a smaller contribution to the mean, at 4.76%, during the same period.

The differences between the two data sources became even more pronounced in the hiatus period (i.e., 1999–2012) than they were during the warming period (i.e., 1982–1998) (Figure 1c,d). Over the period of 1999–2012, the TRENDY ensemble produced a smaller contribution for China to the global LAI trend at $7.92 \pm 25.45\%$, while the observed contribution based on remote sensing data was $15.73 \pm 20.90\%$. Between the two data sources, China's contribution to the global mean and IAV derived from the TRENDY ensemble was 6.82% and 0.94%, respectively, whereas the satellite-based products predicted a similar contribution to the IAV, at 6.08%, and greater contribution to the mean, at 6.24%, during the same period.

Next, we analyzed the long-term trends of LAI based on 13 models from TRENDY—namely, CABLE-POP, CLASS-CTEM, CLM5.0, IBIS, ISAM, ISBA, JULES, LPJ, LPX, ORCHIDEEv3, SDGVM, VISIT, and YIBs (Table 1)—and satellite-based products (GIMMS LAI and GLASS LAI) for the globe and China. Despite large variability in the estimated interannual LAI between the satellite-based products, all LAI datasets exhibited increasing trends before and after the late 1990s (Figure 2). The growth rate in global averaged LAI based on the satellite datasets reduced from $0.009 \pm 0.005 \text{ m}^2 \text{ m}^{-2} \text{ yr}^{-1}$ before the late 1990s to $0.005 \pm 0.002 \text{ m}^2 \text{ m}^{-2} \text{ yr}^{-1}$ during the period of 1999–2012 (Figure 2). However, the growth rate in China increased from $0.012 \pm 0.006 \text{ m}^2 \text{ m}^{-2} \text{ yr}^{-1}$ during the period of 1982–1998 to $0.022 \pm 0.011 \text{ m}^2 \text{ m}^{-2} \text{ yr}^{-1}$ after the late 1990s using the same products. This enhanced positive growth rate was also true for the LAI growth rate during the period of 2000–2017 [12].

This study used 13 models from TRENDY to investigate the long-term changes in LAI for the globe and for China. The TRENDY ensemble showed quite similar long-term trends of LAI, with a significant increasing trend from 1982 to the late 1990s, averaged at $0.004 \pm 0.0118 \text{ m}^2 \text{ m}^{-2} \text{ yr}^{-1}$ ($p < 0.05$) and $0.007 \pm 0.029 \text{ m}^2 \text{ m}^{-2} \text{ yr}^{-1}$ ($p < 0.05$) at the global scale and for China, respectively (Figure 2a,b). However, a decreasing growth rate of LAI was simulated by CLASSIC and ISAM for the globe and by CLASSIC, ISAM, and SDGVM for China, during the same period. Nevertheless, the variations among ecosystem models showed substantial variability in the magnitude and sign of the LAI growth rate, particularly over China, although most models simulated consistent-sign LAI trends. Underestimated LAI trends during the warming hiatus period could have been contributed by the negative trends of LAI from LPX, CABLE-POP, and ISBA. Even the largest increases in the LAI growth rate, simulated by LPJ and VISIT, were smaller than the observed growth rate after the late 1990s.

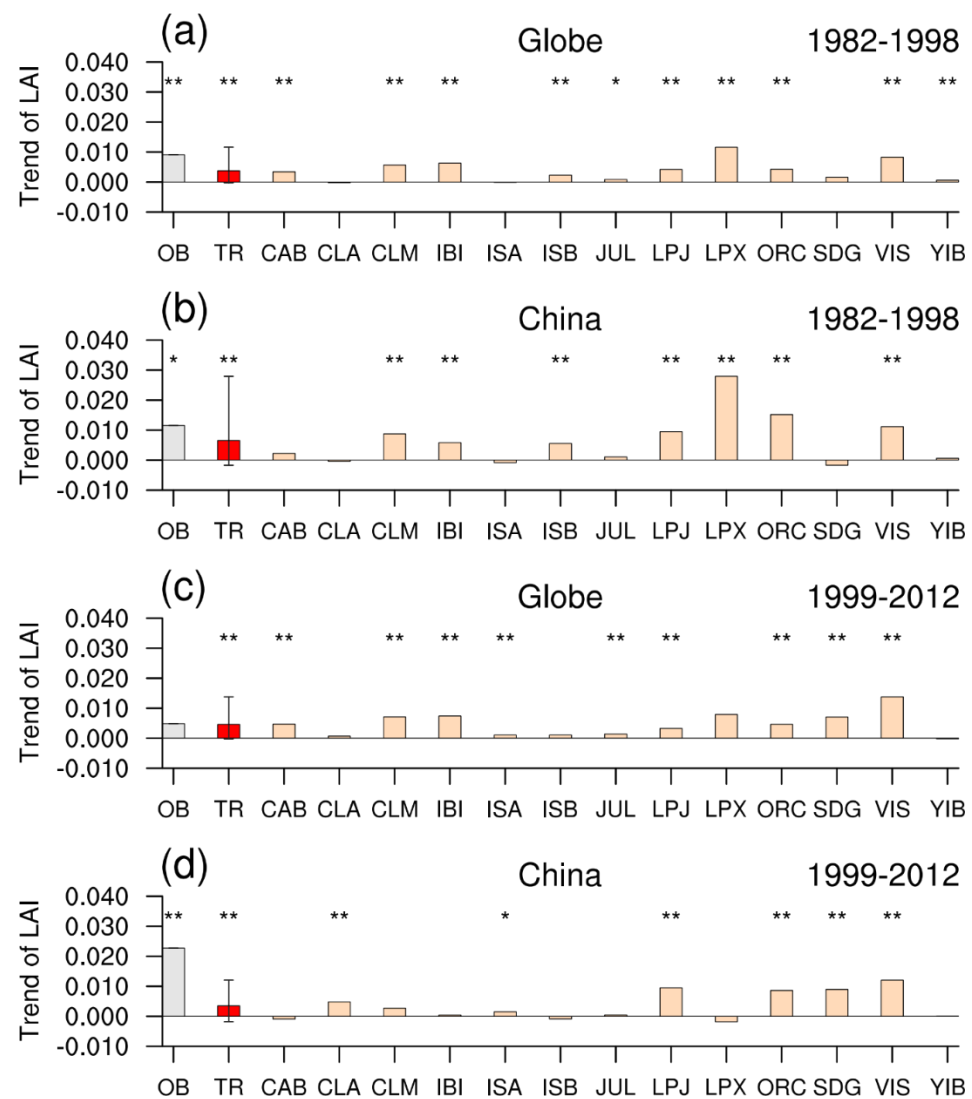


Figure 2. Trends of LAI for the (a,c) globe and (b,d) China during (a,b) the period of 1982–1998 and (c,d) 1999–2012, derived from satellite observation (OB) and 13 TRENDY models. TR means the average of the TRENDY models. Horizontal lines indicate $\pm\sigma$. Two asterisks indicate that the trend is statistically significant ($p < 0.05$) and one asterisk indicates statistical significance at the 0.1 level.

3.2. Responses of LAI Trends to Atmospheric CO₂, Climate, and Land-Use Change

We estimated the impact of climate change, atmospheric CO₂ concentration, and land-use change (Figure 3) on the LAI trends for both the globe and China. With increasing atmospheric CO₂ concentration, the TRENDY ensemble predicted similar magnitudes of increases in LAI trends from 1982 to 1998 for the globe and China. It simulated greater increases in the LAI trend from 1999 to 2012 for China (at $0.0054 \pm 0.004 \text{ m}^2 \text{ m}^{-2} \text{ yr}^{-1}$) than it did for the globe (at $0.0048 \pm 0.003 \text{ m}^2 \text{ m}^{-2} \text{ yr}^{-1}$). Moreover, both the globe and China had greater increases in their LAI trends during the period of 1999–2012 than they did for 1982–1998.

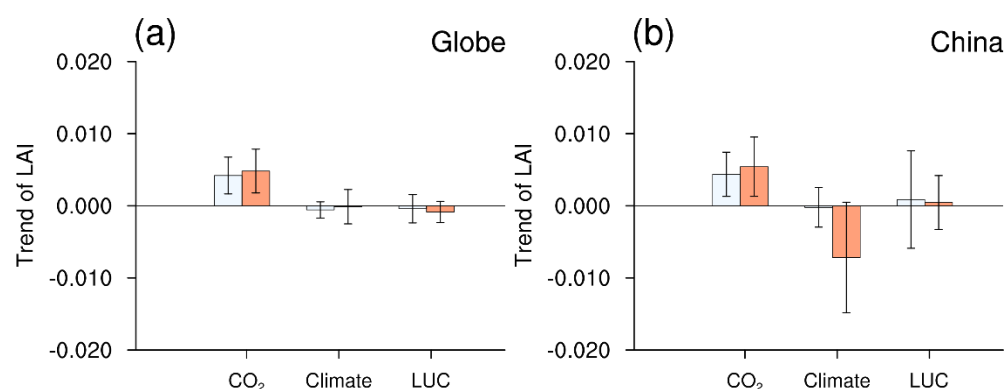


Figure 3. (a,b) Trends in averaged LAI derived from TRENDY models driven by rising CO₂ concentrations (CO₂), climate change (Climate), and land-use change (LUC). Horizontal lines indicate $\pm\sigma$.

In contrast, the responses of the LAI trend to climate change simulated by the TRENDY ensemble differed considerably in both direction and magnitude for the globe and China, as compared with the response to atmospheric CO₂ (Figure 3a,b). The TRENDY ensemble predicted a decrease in the LAI trend by $-0.001 \pm 0.001 \text{ m}^2 \text{ m}^{-2} \text{ yr}^{-1}$ for the globe and $-0.0002 \pm 0.003 \text{ m}^2 \text{ m}^{-2} \text{ yr}^{-1}$ for China during the period of 1982–1998 and by $-0.0001 \pm 0.002 \text{ m}^2 \text{ m}^{-2} \text{ yr}^{-1}$ for the globe and $-0.007 \pm 0.008 \text{ m}^2 \text{ m}^{-2} \text{ yr}^{-1}$ for China during 1999–2012. The simulated responses of the LAI trend to climate change differed significantly in magnitude for China between the two periods. For example, the decreasing LAI trend in China from 1999 to 2012 was simulated to have been more than 32 times greater than that from 1982 to 1998.

For China, the TRENDY ensemble simulated a much greater decrease in the LAI trend than it did for the globe. Climate change was the most important mechanism for this simulated decrease in the LAI trend across China during the hiatus period of 1999–2012 (Figure 3b). Surface air temperature and precipitation are the most important factors regulating LAI. Most vegetation growth and productivity over land is determined by these two factors, both globally and in specific regions [10,40–42]. For example, high precipitation was found to contribute about 12%, thereby helping to offset land-to-atmosphere CO₂ fluxes driven by long-term negative temperature and direct radiative contributions [28]. In addition, some studies have reported the importance of VPD will increase under the warming climate [43–45].

3.3. Implications of Climatic Variables for Estimated LAI Trends

Based on CRUNCEP data, Figure 4 illustrates that precipitation in China decreased from 1999 to 2012 ($y = -0.14x + 3.29$, $p = 0.07$), while the precipitation trend from 1982 to 1998 remained non-significant ($y = 0.04x - 0.35$, $p = 0.43$). From 1982 to 1998, the globe showed a slight increasing trend in precipitation ($y = 0.03x - 0.56$, $p = 0.56$), and a similar trend was found for the globe during 1999–2012 ($y = 0.02x + 0.01$, $p = 0.74$). The trend of air temperature over land after 1999 was lower than that from 1982 to 1998 over globally vegetated areas. China showed a decreasing trend in air temperature ($y = -0.03x + 1.57$, $p = 0.29$). Before 1999, decreasing trends of total incident solar radiation over both the globe and China were revealed, while an increase in total incident solar radiation was shown during the period of 1999–2012. However, as a result of global warming, the VPD globally and over China increased significantly by 0.028 and $0.051 \text{ hPa yr}^{-1}$ ($p < 0.05$), respectively, during the period of 1999–2012 compared with the period of 1982–1998 (Figure 5).

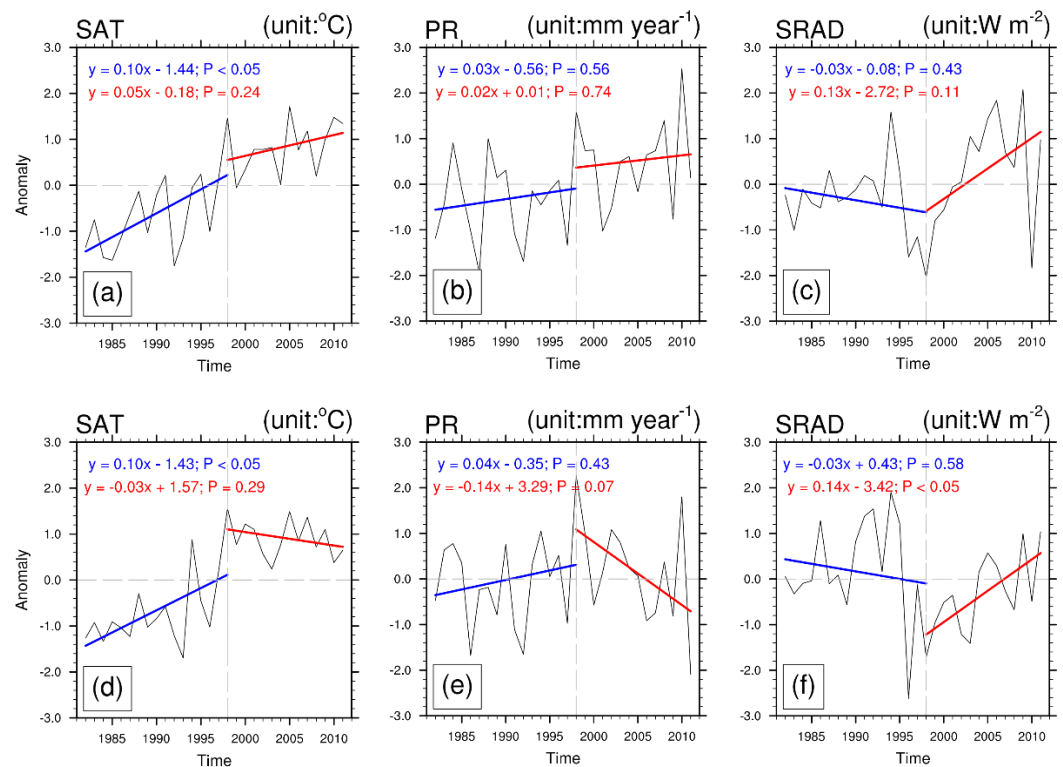


Figure 4. Changes in growing-season-average climate drivers (SAT: surface air temperature; PR: precipitation; SRAD: solar radiation) for the (a–c) whole terrestrial ecosystem and (d–f) China over the period of 1982–1998 (red) and 1999–2012 (blue), where SAT, PR or SRAD (y) is calculated by the time (x) using a linear regression, p represents significant level.

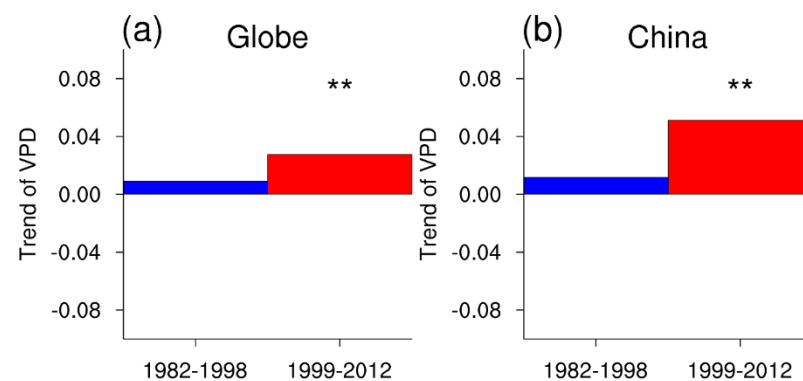


Figure 5. (a) Trends of atmospheric vapor pressure deficit (VPD) (unit: hPa yr⁻¹) for (a) the globe and (b) China. Two asterisks indicate that the trend is statistically significant ($p < 0.05$).

To quantify the underestimation of the LAI trend simulated by the TRENDY ensemble, we further explored the LAI sensitivity to climate variables (i.e., air temperature, precipitation, shortwave radiation, and VPD) using the simulations of S2 minus S1 from 1999 to 2012, compared with those during the period of 1982–1998. The simulation-based datasets showed similar LAI sensitivity to VPD, whereby a decrease in LAI for China was shown (average of $-0.058 \text{ m}^2 \text{ m}^{-2}$ ranging from -0.177 to $0.006 \text{ m}^2 \text{ m}^{-2}$, with a VPD increase of 1 hPa) during the warming hiatus (Figure 6), which was opposite to that during the warming period (average of $0.039 \text{ m}^2 \text{ m}^{-2}$ ranging from -0.009 to $0.172 \text{ m}^2 \text{ m}^{-2}$, with a VPD increase of 1 hPa).

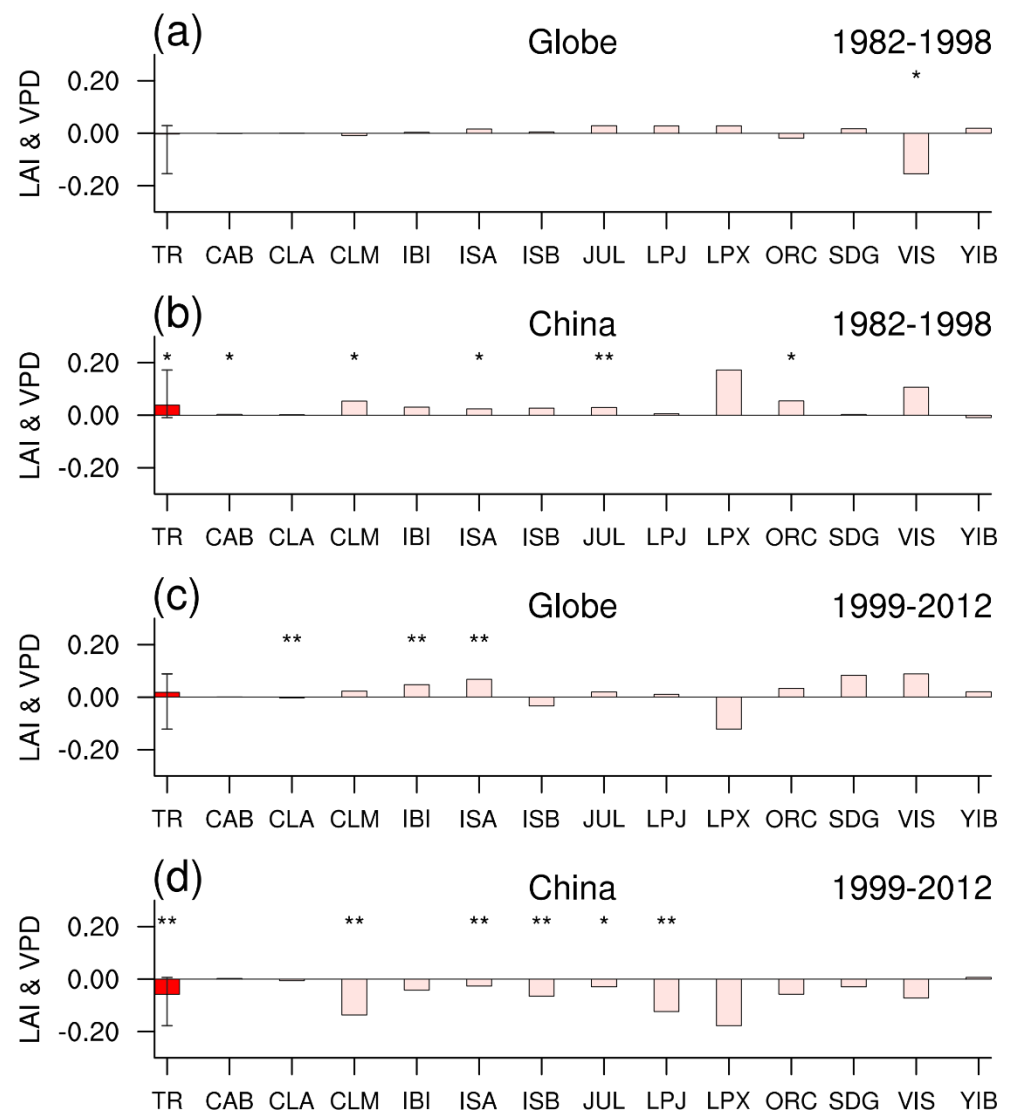


Figure 6. Sensitivities of LAI to VPD during the growing season for (a,c) the globe and (b,d) China during (a,b) 1982–1998 and (c,d) 1999–2012, derived from 13 TRENDY models (unit: $(\text{hPa})^{-1}$). TR means the average of TRENDY models. Horizontal lines indicate $\pm\sigma$. Two asterisks indicate that the trend is statistically significant ($p < 0.05$) and one asterisk indicates statistical significance at the 0.1 level.

However, faintly positive sensitivities of global LAI to VPD were apparent before the late 1990s but did not pass at the 5% level using the Mann–Kendall test ($p > 0.05$). Most TRENDY models showed stronger positive responses afterwards. Thus, a negative impact on LAI of the significantly enhanced VPD from 1999 to 2012 was shown at the global scale. On the basis of the estimated LAI sensitivity, we also estimated the contributions of surface air temperature and precipitation to global LAI over the two study periods (Figures S1 and S2). Only a few models showed significant LAI sensitivity to these three climatic variables.

3.4. Implications of Land-Use Change for Estimated LAI Trends

In both periods, the simulated LAI trends from terrestrial ecosystem models were less responsive to changes in land use than they were to atmospheric CO_2 or climate change. Changes in land use caused the LAI trend to decrease for the globe but resulted in an increase in the LAI trend for China (Figure 3). To report the uncertainty in our estimate, we used a range of ± 1 standard deviation (σ) [24], revealing that the standard deviation of the trend in LAI for China across ecosystem models was ± 0.007 and $\pm 0.004 \text{ m}^2 \text{ m}^{-2} \text{ yr}^{-1}$

before and after the late 1990s, respectively. Although the uncertainty in every aspect for China was large (e.g., climate change), the uncertainty of land use in China’s LAI trends in the past 30 years was the greatest in terms of the magnitude and sign of each TRENDY model (Figure 7). This is because land-use and land-cover datasets are inherently uncertain in China, just as they are in other parts of the world, as concluded by Piao et al., (2018) [6].

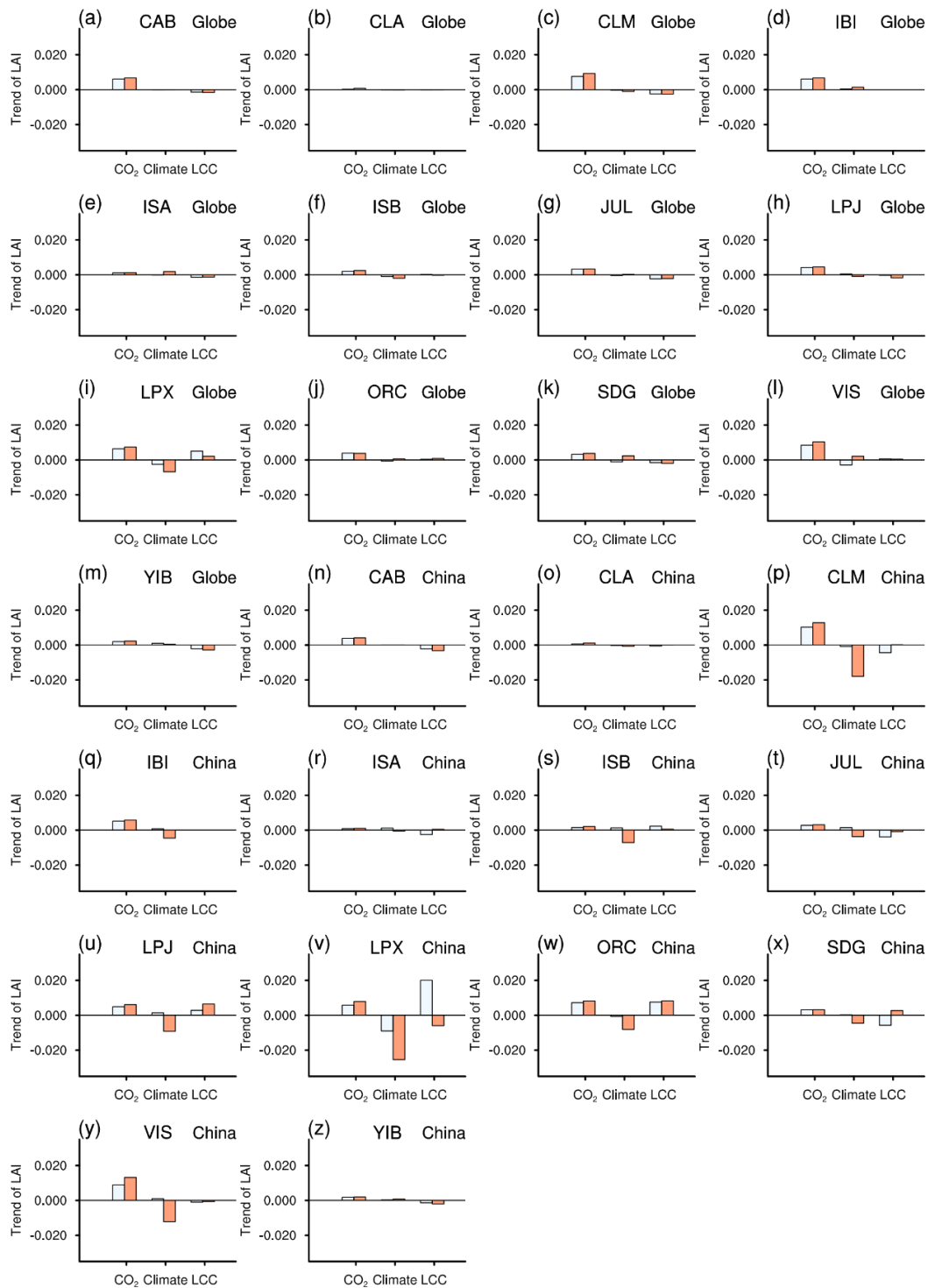


Figure 7. Trends in averaged LAI derived from each TRENDY model driven by rising CO₂ concentrations (CO₂), climate change (Climate), and land-use change (LUC) for the globe in (a–m) and China in (n–z).

4. Discussion

We have examined whether terrestrial ecosystem models can adequately capture the observed enhanced contribution of China to the global increasing trend in LAI after the late 1990s, based on results from 13 such models. We found that the simulated LAI trends of most models did not match the satellite LAI trends for China. Only the LPJ, ORCHIDEE, SDGVM, and VISIT models showed greater increasing LAI trends after the late 1990s, similar to the satellite-based LAI trend estimates (Figure 2). The terrestrial ecosystem models showed a smaller contribution of China to the global increasing LAI trend than did the satellite-based datasets, with a reduction of ~7.81%.

In one respect, our results support an underestimation of China's contribution to the global LAI trend during the warming hiatus, which has been observed as an enhanced contribution during the same period. The significantly increased VPD might have strengthened the negative climatic impact on the LAI trend for China. Owing to the high evaporative demand of the air, an increasing trend of VPD (Figure 5) might prompt enhanced stomatal closure, which can help to avoid excess water loss [46]. Carbohydrate reserves are depleted and tissue-level carbohydrate starvation can be caused by such enhanced stomatal closure [47]. Thus, plant growth, production, and respiration become restricted [16,48,49]. Indeed, enhanced VPD in the southwestern United States has been shown to determine warm-season drought linked to dehydrated plant tissues and reduced plant productivity, thereby leading to increased plant mortality [50]. In addition, during the hiatus period with a warmer climate, the negative contributions of VPD for China were likely enhanced, resulting from stomatal regulation [44,45]. Plus, it is difficult to isolate the relative contributions of higher VPD from the combined climatic impact, including warmer temperatures and the decreasing trend in precipitation for China.

Our results imply that most terrestrial ecosystem models cannot capture negative LAI trend responses to enhanced VPD at the global scale (Figure 6). The globally averaged sensitivity of LAI to VPD simulated by TRENDY was positive, at $\sim 0.018 \pm 0.053$. The sign of the sensitivity differed from the previous estimation by Yuan et al. [16], possibly indicating a mismatch between the models used in this study and observations with respect to the relationship between LAI and enhanced VPD. The results of our analysis suggest that an area for future model improvements is the negative impact of enhanced VPD on vegetation.

In another respect, other problems in reproducing the observed reduced increasing LAI trend responses to CO₂ concentrations may challenge the ability of models to predict vegetation states. Models participating in the TRENDY project (Table 1) predicted a continuous increase in the LAI trend during the warming hiatus due to CO₂ fertilization effects (Figures 3 and 7). However, a recent study using multiple long-term satellite- and ground-based datasets [51] showed that global CO₂ fertilization effects declined across most terrestrial regions of the globe. Regarding these two aspects, the responses of global LAI trends to increased VPD and CO₂ concentrations might explain why there is no underestimation at the global scale compared with the observed increasing LAI trend. At the global scale, our results suggest that most terrestrial ecosystem models cannot well reproduce in both direction and magnitude of vegetation responses to VPD (Figure 6). Thus, this predicted negative impact on vegetation growth considerably results from increasing VPD, which must be inspected cautiously when estimating the regional contribution to global greening.

Finally, it is important to highlight that uncertainties remain in terms of the magnitude of the sensitivity of LAI to land-use change for terrestrial ecosystem models [52]. The impacts of land-use change on LAI trends depend crucially on the regional climate, prior land cover, and scale of management [53,54]. Afforestation in China will have larger positive impacts than at the global scale because of the intensive ecosystem management in China. Recently, it was reported that China alone accounts for 25% of the global net increase in leaf area, with only 6.6% of the global vegetated area according to satellite data [12]. However, growth rates of LAI can be dampened or enhanced by changes in local land cover and land use (e.g., for China) in the second period, as derived from ecosystem models

(Figure 7). In total, 7 out of 13 ecosystem models show a negative impact of land-use changes on LAI trends for China, in contrast to satellite-based LAI estimates [12]. It should be noted that a few models are now capable of considering other human land-use management factors such as forest management and changes in cultivation practices, crop varieties, and phosphorus and potassium limitations [1]. For China, the lack of these factors in ecosystem models might be a cause of the mismatch between observed and simulated LAI trends.

5. Conclusions

This study investigated the regulation by different drivers of China's contribution to the global trend in LAI. The results show that current terrestrial models have poor ability in reproducing China's contribution to global greening. In particular, China's contribution to global greening from 1999 to 2012 has been underestimated by ~7.81% (Figure 8). Climate changes dominate this underestimation of China's contribution. Explicitly, global VPD substantially increased after 1999. Conversely, current terrestrial models did not well reproduce global vegetation growth responses to continuously increasing VPD after 1999. In addition, our results show a poor ability of current terrestrial models in reproducing the positive impact of land-use changes (i.e., afforestation) on vegetation growth for China. Generally, this study highlights the dominant role of both VPD and land-use change on China's contribution to the global greening.

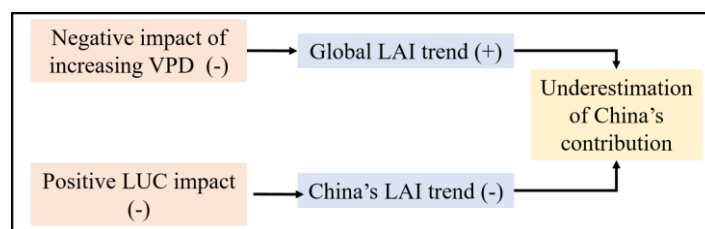


Figure 8. A schematic diagram of the underestimation of China's contribution to global greening by terrestrial ecosystem models during the period of 1999–2012. On the one hand, the negative effect of a rapid increase in VPD on global LAI trends was underestimated by terrestrial ecosystem models. On the other hand, the positive impact of afforestation in China has been underestimated or ignored in the terrestrial ecosystem model. These have led to an underestimation of China's contribution to global greening. Symbols (+ or −) indicate an increase or decrease in the variable's effect on the increasing trend of LAI, respectively.

Supplementary Materials: The following supporting information can be downloaded at: <https://www.mdpi.com/article/10.3390/land11030393/s1>, Figure S1: Sensitivities of LAI to surface air temperature (SAT) during the growing season for (a,c) the globe and (b,d) China during (a,b) 1982–1998 and (c,d) 1999–2012, derived from 13 TRENDY models (unit: $^{\circ}\text{C}^{-1}$). TR means the average of TRENDY models. Horizontal lines indicate $\pm\sigma$. Two asterisks indicate that the trend is statistically significant ($p < 0.05$) and one asterisks indicates statistical significance at the 0.1 level.; Figure S2: Sensitivities of LAI to precipitation (PR) during the growing season for (a,c) the globe and (b,d) China during (a,b) 1982–1998 and (c,d) 1999–2012, derived from 13 TRENDY models (unit: $0.01 \text{ mm}^{-1} \text{ year}$). TR means the average of TRENDY models. Horizontal lines indicate $\pm\sigma$. Two asterisks indicate that the trend is statistically significant ($p < 0.05$) and one asterisks indicates statistical significance at the 0.1 level.

Author Contributions: Conceptualization, J.P.; methodology, J.P.; software, F.Y.; formal analysis, L.D. and X.T.; data curation, F.Y.; writing—original draft preparation, J.P.; writing—review and editing, J.P.; visualization, J.P., X.T. and F.Y.; supervision, L.D.; project administration, L.D.; funding acquisition, L.D. All authors have read and agreed to the published version of the manuscript.

Funding: This research was funded by projects of the National Natural Science Foundation of China (Grant Nos. 41630532, 41975112, 42175142, 42175013, 42141017).

Institutional Review Board Statement: Not applicable.

Informed Consent Statement: Not applicable.

Data Availability Statement: All supporting data are cited within the Section 2 Materials and Methods.

Acknowledgments: We thanks for the four peer reviewers selected by the journal for their feedback and input, as well as Colin Smith from LucidPapers to edit our manuscript.

Conflicts of Interest: The authors declare no conflict of interest.

References

- Zhu, Z.; Piao, S.; Myneni, R.B.; Huang, M.; Zeng, Z.; Canadell, J.G.; Ciais, P.; Sitch, S.; Friedlingstein, P.; Arneeth, A.; et al. Greening of the Earth and its drivers. *Nat. Clim. Change* **2016**, *6*, 791–795. [[CrossRef](#)]
- Zhao, Z.-Q.; He, B.-J.; Li, L.-G.; Wang, H.-B.; Darko, A. Profile and concentric zonal analysis of relationships between land use/land cover and land surface temperature: Case study of Shenyang, China. *Energy Build.* **2017**, *155*, 282–295. [[CrossRef](#)]
- Zhao, Z.; Sharifi, A.; Dong, X.; Shen, L.; He, B.-J. Spatial Variability and Temporal Heterogeneity of Surface Urban Heat Island Patterns and the Suitability of Local Climate Zones for Land Surface Temperature Characterization. *Remote Sens.* **2021**, *13*, 4338. [[CrossRef](#)]
- Zhu, Z.; Bi, J.; Pan, Y.; Ganguly, S.; Anav, A.; Xu, L.; Samanta, A.; Piao, S.; Nemani, R.R.; Myneni, R.B. Global Data Sets of Vegetation Leaf Area Index (LAI)3g and Fraction of Photosynthetically Active Radiation (FPAR)3g Derived from Global Inventory Modeling and Mapping Studies (GIMMS) Normalized Difference Vegetation Index (NDVI3g) for the Period 1981 to 2011. *Remote Sens.* **2013**, *5*, 927. [[CrossRef](#)]
- Anav, A.; Murray-Tortarolo, G.; Friedlingstein, P.; Sitch, S.; Piao, S.; Zhu, Z. Evaluation of Land Surface Models in Reproducing Satellite Derived Leaf Area Index over the High-Latitude Northern Hemisphere. Part II: Earth System Models. *Remote Sens.* **2013**, *5*, 3637. [[CrossRef](#)]
- Piao, S.; Huang, M.; Liu, Z.; Wang, X.; Ciais, P.; Canadell, J.G.; Wang, K.; Bastos, A.; Friedlingstein, P.; Houghton, R.A.; et al. Lower land-use emissions responsible for increased net land carbon sink during the slow warming period. *Nat. Geosci.* **2018**, *11*, 739–743. [[CrossRef](#)]
- Park, T.; Chen, C.; Macias-Fauria, M.; Tømmervik, H.; Choi, S.; Winkler, A.; Bhatt, U.S.; Walker, D.A.; Piao, S.; Brovkin, V.; et al. Changes in timing of seasonal peak photosynthetic activity in northern ecosystems. *Global Change Biol.* **2019**, *25*, 2382–2395. [[CrossRef](#)]
- Mahowald, N.; Lo, F.; Zheng, Y.; Harrison, L.; Funk, C.; Lombardozzi, D.; Goodale, C. Projections of leaf area index in earth system models. *Earth Syst. Dynam.* **2016**, *7*, 211–229. [[CrossRef](#)]
- Huntzinger, D.N.; Michalak, A.M.; Schwalm, C.; Ciais, P.; King, A.W.; Fang, Y.; Schaefer, K.; Wei, Y.; Cook, R.B.; Fisher, J.B.; et al. Uncertainty in the response of terrestrial carbon sink to environmental drivers undermines carbon-climate feedback predictions. *Sci. Rep.* **2017**, *7*, 4765. [[CrossRef](#)]
- Piao, S.; Wang, X.; Park, T.; Chen, C.; Lian, X.; He, Y.; Bjerke, J.W.; Chen, A.; Ciais, P.; Tømmervik, H.; et al. Characteristics, drivers and feedbacks of global greening. *Nat. Rev. Earth Environ.* **2020**, *1*, 14–27. [[CrossRef](#)]
- Mao, J.; Ribes, A.; Yan, B.; Shi, X.; Thornton, P.E.; Séférian, R.; Ciais, P.; Myneni, R.B.; Douville, H.; Piao, S.; et al. Human-induced greening of the northern extratropical land surface. *Nat. Clim. Change* **2016**, *6*, 959–963. [[CrossRef](#)]
- Chen, C.; Park, T.; Wang, X.; Piao, S.; Xu, B.; Chaturvedi, R.K.; Fuchs, R.; Brovkin, V.; Ciais, P.; Fensholt, R.; et al. China and India lead in greening of the world through land-use management. *Nat. Sustain.* **2019**, *2*, 122–129. [[CrossRef](#)] [[PubMed](#)]
- Zeng, Z.; Zhu, Z.; Lian, X.; Li, L.Z.X.; Chen, A.; He, X.; Piao, S. Responses of land evapotranspiration to Earth's greening in CMIP5 Earth System Models. *Environ. Res. Lett.* **2016**, *11*, 104006. [[CrossRef](#)]
- Medhaug, I.; Stolpe, M.B.; Fischer, E.M.; Knutti, R. Reconciling controversies about the 'global warming hiatus'. *Nature* **2017**, *545*, 41–47. [[CrossRef](#)] [[PubMed](#)]
- Ballantyne, A.; Smith, W.; Anderegg, W.; Kauppi, P.; Sarmiento, J.; Tans, P.; Shevliakova, E.; Pan, Y.; Poulter, B.; Anav, A.; et al. Accelerating net terrestrial carbon uptake during the warming hiatus due to reduced respiration. *Nat. Clim. Change* **2017**, *7*, 148–152. [[CrossRef](#)]
- Yuan, W.; Zheng, Y.; Piao, S.; Ciais, P.; Lombardozzi, D.; Wang, Y.; Ryu, Y.; Chen, G.; Dong, W.; Hu, Z.; et al. Increased atmospheric vapor pressure deficit reduces global vegetation growth. *Sci. Adv.* **2019**, *5*, eaax1396. [[CrossRef](#)]
- Cortés, J.; Mahecha, M.D.; Reichstein, M.; Myneni, R.B.; Chen, C.; Brenning, A. Where Are Global Vegetation Greening and Browning Trends Significant? *Geophys. Res. Lett.* **2021**, *48*, e2020GL091496. [[CrossRef](#)]
- Piao, S.; Wang, X.; Wang, K.; Li, X.; Bastos, A.; Canadell, J.G.; Ciais, P.; Friedlingstein, P.; Sitch, S. Interannual variation of terrestrial carbon cycle: Issues and perspectives. *Global Change Biol.* **2020**, *26*, 300–318. [[CrossRef](#)]
- Haverd, V.; Smith, B.; Nieradzick, L.; Briggs, P.R.; Woodgate, W.; Trudinger, C.M.; Canadell, J.G.; Cuntz, M. A new version of the CABLE land surface model (Subversion revision r4601) incorporating land use and land cover change, woody vegetation demography, and a novel optimisation-based approach to plant coordination of photosynthesis. *Geosci. Model Dev.* **2018**, *11*, 2995–3026. [[CrossRef](#)]
- Melton, J.R.; Arora, V.K. Competition between plant functional types in the Canadian Terrestrial Ecosystem Model (CTEM) v. 2.0. *Geosci. Model Dev.* **2016**, *9*, 323–361. [[CrossRef](#)]

21. Meiyappan, P.; Jain, A.K.; House, J.I. Increased influence of nitrogen limitation on CO₂ emissions from future land use and land use change. *Glob. Biogeochem. Cycles* **2015**, *29*, 1524–1548. [[CrossRef](#)]
22. Delire, C.; Séférian, R.; Decharme, B.; Alkama, R.; Calvet, J.-C.; Carrer, D.; Gibelin, A.-L.; Joetzjer, E.; Morel, X.; Rocher, M.; et al. The Global Land Carbon Cycle Simulated With ISBA-CTRIP: Improvements Over the Last Decade. *J. Adv. Model. Earth Syst.* **2020**, *12*, e2019MS001886. [[CrossRef](#)]
23. Clark, D.B.; Mercado, L.M.; Sitch, S.; Jones, C.D.; Gedney, N.; Best, M.J.; Pryor, M.; Rooney, G.G.; Essery, R.L.H.; Blyth, E.; et al. The Joint UK Land Environment Simulator (JULES), model description—Part 2: Carbon fluxes and vegetation dynamics. *Geosci. Model Dev.* **2011**, *4*, 701–722. [[CrossRef](#)]
24. Poulter, B.; Cadule, P.; Cheiney, A.; Ciais, P.; Hodson, E.; Peylin, P.; Plummer, S.; Spessa, A.; Saatchi, S.; Yue, C.; et al. Sensitivity of global terrestrial carbon cycle dynamics to variability in satellite-observed burned area. *Glob. Biogeochem. Cycles* **2015**, *29*, 207–222. [[CrossRef](#)]
25. Prentice, I.C.; Kelley, D.I.; Foster, P.N.; Friedlingstein, P.; Harrison, S.P.; Bartlein, P.J. Modeling fire and the terrestrial carbon balance. *Glob. Biogeochem. Cycles* **2011**, *25*, GB3005. [[CrossRef](#)]
26. Krinner, G.; Viovy, N.; de Noblet-Ducoudré, N.; Ogee, J.; Polcher, J.; Friedlingstein, P.; Ciais, P.; Sitch, S.; Prentice, I.C. A dynamic global vegetation model for studies of the coupled atmosphere-biosphere system. *Glob. Biogeochem. Cycles* **2005**, *19*, GB1015. [[CrossRef](#)]
27. Walker, A.P.; Quaipe, T.; van Bodegom, P.M.; De Kauwe, M.G.; Keenan, T.F.; Joiner, J.; Lomas, M.R.; MacBean, N.; Xu, C.; Yang, X.; et al. The impact of alternative trait-scaling hypotheses for the maximum photosynthetic carboxylation rate (V_{cmax}) on global gross primary production. *New Phytol.* **2017**, *215*, 1370–1386. [[CrossRef](#)]
28. Kato, E.; Kinoshita, T.; Ito, A.; Kawamiya, M.; Yamagata, Y. Evaluation of spatially explicit emission scenario of land-use change and biomass burning using a process-based biogeochemical model. *J. Land Use Sci.* **2013**, *8*, 104–122. [[CrossRef](#)]
29. Tian, C.; Yue, X.; Zhou, H.; Lei, Y.; Ma, Y.; Cao, Y. Projections of changes in ecosystem productivity under 1.5 °C and 2 °C global warming. *Glob. Planet. Change* **2021**, *205*, 103588. [[CrossRef](#)]
30. Le Quéré, C.; Andrew, R.M.; Friedlingstein, P.; Sitch, S.; Hauck, J.; Pongratz, J.; Pickers, P.A.; Korsbakken, J.I.; Peters, G.P.; Canadell, J.G.; et al. Global Carbon Budget 2018. *Earth Syst. Sci. Data* **2018**, *10*, 2141–2194. [[CrossRef](#)]
31. Sitch, S.; Friedlingstein, P.; Gruber, N.; Jones, S.D.; Murray-Tortarolo, G.; Ahlström, A.; Doney, S.C.; Graven, H.; Heinze, C.; Huntingford, C.; et al. Recent trends and drivers of regional sources and sinks of carbon dioxide. *Biogeosciences* **2015**, *12*, 653–679. [[CrossRef](#)]
32. Bonan, G.B.; Lombardozzi, D.L.; Wieder, W.R.; Oleson, K.W.; Lawrence, D.M.; Hoffman, F.M.; Collier, N. Model Structure and Climate Data Uncertainty in Historical Simulations of the Terrestrial Carbon Cycle (1850–2014). *Glob. Biogeochem. Cycles* **2019**, *33*, 1310–1326. [[CrossRef](#)]
33. Ahlström, A.; Raupach Michael, R.; Schurgers, G.; Smith, B.; Arneeth, A.; Jung, M.; Reichstein, M.; Canadell Josep, G.; Friedlingstein, P.; Jain Atul, K.; et al. The dominant role of semi-arid ecosystems in the trend and variability of the land CO₂ sink. *Science* **2015**, *348*, 895–899. [[CrossRef](#)] [[PubMed](#)]
34. Piao, S.; Sitch, S.; Ciais, P.; Friedlingstein, P.; Peylin, P.; Wang, X.; Ahlström, A.; Anav, A.; Canadell, J.G.; Cong, N.; et al. Evaluation of terrestrial carbon cycle models for their response to climate variability and to CO₂ trends. *Glob. Change Biol.* **2013**, *19*, 2117–2132. [[CrossRef](#)] [[PubMed](#)]
35. Fernández-Martínez, M.; Sardans, J.; Chevallier, F.; Ciais, P.; Obersteiner, M.; Vicca, S.; Canadell, J.G.; Bastos, A.; Friedlingstein, P.; Sitch, S.; et al. Global trends in carbon sinks and their relationships with CO₂ and temperature. *Nat. Clim. Change* **2019**, *9*, 73–79. [[CrossRef](#)]
36. Bastos, A.; O’Sullivan, M.; Ciais, P.; Makowski, D.; Sitch, S.; Friedlingstein, P.; Chevallier, F.; Rödenbeck, C.; Pongratz, J.; Luijckx, I.T.; et al. Sources of Uncertainty in Regional and Global Terrestrial CO₂ Exchange Estimates. *Glob. Biogeochem. Cycles* **2020**, *34*, e2019GB006393. [[CrossRef](#)]
37. Piao, S.; Tan, J.; Chen, A.; Fu, Y.H.; Ciais, P.; Liu, Q.; Janssens, I.A.; Vicca, S.; Zeng, Z.; Jeong, S.-J.; et al. Leaf onset in the northern hemisphere triggered by daytime temperature. *Nat. Commun.* **2015**, *6*, 6911. [[CrossRef](#)]
38. Alduchov, O.A.; Eskridge, R.E. Improved Magnus Form Approximation of Saturation Vapor Pressure. *J. Appl. Meteorol. Climatol.* **1996**, *35*, 601–609. [[CrossRef](#)]
39. Poulter, B.; Frank, D.; Ciais, P.; Myneni, R.B.; Andela, N.; Bi, J.; Broquet, G.; Canadell, J.G.; Chevallier, F.; Liu, Y.Y.; et al. Contribution of semi-arid ecosystems to interannual variability of the global carbon cycle. *Nature* **2014**, *509*, 600–603. [[CrossRef](#)]
40. Peng, J.; Dan, L.; Yang, F.; Tang, X.; Wang, D. Global and regional estimation of carbon uptake using CMIP6 ESM compared with TRENDY ensembles at the centennial scale. *J. Geophys. Res. Atmos.* **2021**, *126*, e2021JD035135. [[CrossRef](#)]
41. Peng, J.; Dan, L.; Ying, K.; Yang, S.; Tang, X.; Yang, F. China’s Interannual Variability of Net Primary Production Is Dominated by the Central China Region. *J. Geophys. Res. Atmos.* **2021**, *126*, e2020JD033362. [[CrossRef](#)]
42. Piao, S.; Ciais, P.; Friedlingstein, P.; Noblet-Ducoudré, N.d.; Cadule, P.; Viovy, N.; Wang, T. Spatiotemporal patterns of terrestrial carbon cycle during the 20th century. *Glob. Biogeochem. Cycles* **2009**, *23*, GB4026. [[CrossRef](#)]
43. Ficklin, D.L.; Novick, K.A. Historic and projected changes in vapor pressure deficit suggest a continental-scale drying of the United States atmosphere. *J. Geophys. Res. Atmos.* **2017**, *122*, 2061–2079. [[CrossRef](#)]
44. Grossiord, C.; Buckley, T.N.; Cernusak, L.A.; Novick, K.A.; Poulter, B.; Siegwolf, R.T.W.; Sperry, J.S.; McDowell, N.G. Plant responses to rising vapor pressure deficit. *New Phytol.* **2020**, *226*, 1550–1566. [[CrossRef](#)]

45. Novick, K.A.; Ficklin, D.L.; Stoy, P.C.; Williams, C.A.; Bohrer, G.; Oishi, A.C.; Papuga, S.A.; Blanken, P.D.; Noormets, A.; Sulman, B.N.; et al. The increasing importance of atmospheric demand for ecosystem water and carbon fluxes. *Nat. Clim. Change* **2016**, *6*, 1023–1027. [[CrossRef](#)]
46. McAdam, S.A.; Sussmilch, F.C.; Brodribb, T.J. Stomatal responses to vapour pressure deficit are regulated by high speed gene expression in angiosperms. *Plant Cell Environ.* **2016**, *39*, 485–491. [[CrossRef](#)]
47. McDowell, N.; Pockman, W.T.; Allen, C.D.; Breshears, D.D.; Cobb, N.; Kolb, T.; Plaut, J.; Sperry, J.; West, A.; Williams, D.G.; et al. Mechanisms of plant survival and mortality during drought: Why do some plants survive while others succumb to drought? *New Phytol.* **2008**, *178*, 719–739. [[CrossRef](#)]
48. Menezes-Silva, P.E.; Loram-Lourenço, L.; Alves, R.D.F.B.; Sousa, L.F.; Almeida, S.E.d.S.; Farnese, F.S. Different ways to die in a changing world: Consequences of climate change for tree species performance and survival through an ecophysiological perspective. *Ecol. Evol.* **2019**, *9*, 11979–11999. [[CrossRef](#)]
49. Liu, L.; Gudmundsson, L.; Hauser, M.; Qin, D.; Li, S.; Seneviratne, S.I. Soil moisture dominates dryness stress on ecosystem production globally. *Nat. Commun.* **2020**, *11*, 4892. [[CrossRef](#)]
50. Koster, R.D.; Suarez, M.J.; Heiser, M. Variance and Predictability of Precipitation at Seasonal-to-Interannual Timescales. *J. Hydrol.* **2000**, *1*, 26–46. [[CrossRef](#)]
51. Wang, S.; Zhang, Y.; Ju, W.; Chen, J.M.; Ciais, P.; Cescatti, A.; Sardans, J.; Janssens, I.A.; Wu, M.; Berry, J.A.; et al. Recent global decline of CO₂ fertilization effects on vegetation photosynthesis. *Science* **2020**, *370*, 1295. [[CrossRef](#)] [[PubMed](#)]
52. Zhao, D.; Wang, J.; Zhao, X.; Triantafyllidis, J. Clay content mapping and uncertainty estimation using weighted model averaging. *CATENA* **2022**, *209*, 105791. [[CrossRef](#)]
53. Trabucco, A.; Zomer, R.J.; Bossio, D.A.; van Straaten, O.; Verchot, L.V. Climate change mitigation through afforestation/reforestation: A global analysis of hydrologic impacts with four case studies. *Agric. Ecosyst. Environ.* **2008**, *126*, 81–97. [[CrossRef](#)]
54. Malone, B.P.; Minasny, B.; Odgers, N.P.; McBratney, A.B. Using model averaging to combine soil property rasters from legacy soil maps and from point data. *Geoderma* **2014**, *232–234*, 34–44. [[CrossRef](#)]